Transient Potential Gradients and Impedance Measures of Tethered Bilayer Lipid Membranes: Pore-Forming Peptide Insertion and the Effect of Electroporation

Charles G. Cranfield,[†‡*] Bruce A. Cornell,[§] Stephan L. Grage,[¶] Paul Duckworth,[‖] Sonia Carne,[§] Anne S. Ulrich,[¶] and Boris Martinac[†‡]

[†]Molecular Cardiology and Biophysics Division, Victor Chang Cardiac Research Institute, Darlinghurst, New South Wales, Australia; [‡]St. Vincent's Clinical School, University of New South Wales, Sydney, Australia; [§]Surgical Diagnostics, Roseville, New South Wales, Australia; [¶]Karlsruhe Institute of Technology, Institute of Biological Interfaces (IBG-2), Karlsruhe, Germany; and [‖]eDAQ, Denistone East, New South Wales. Australia

ABSTRACT In this work, we present experimental data, supported by a quantitative model, on the generation and effect of potential gradients across a tethered bilayer lipid membrane (tBLM) with, to the best of our knowledge, novel architecture. A challenge to generating potential gradients across tBLMs arises from the tethering coordination chemistry requiring an inert metal such as gold, resulting in any externally applied voltage source being capacitively coupled to the tBLM. This in turn causes any potential across the tBLM assembly to decay to zero in milliseconds to seconds, depending on the level of membrane conductance. Transient voltages applied to tBLMs by pulsed or ramped direct-current amperometry can, however, provide current-voltage (I/V) data that may be used to measure the voltage dependency of the membrane conductance. We show that potential gradients >~150 mV induce membrane defects that permit the insertion of pore-forming peptides. Further, we report here the novel (to our knowledge) use of real-time modeling of conventional low-voltage alternating-current impedance spectroscopy to identify whether the conduction arising from the insertion of a polypeptide is uniform or heterogeneous on scales of nanometers to micrometers across the membrane. The utility of this tBLM architecture and these techniques is demonstrated by characterizing the resulting conduction properties of the antimicrobial peptide PGLa.

INTRODUCTION

Tethered bilayer lipid membranes (tBLMs) typically consist of a lipid bilayer attached by a sulfur-gold chemistry to a thin gold film deposited onto a solid insulating substrate. The advantage of tBLMs is that, unlike patched or so called black lipid membranes (BLMs), tBLMs are stable for months and do not instantaneously fail when subjected to robust mechanical mixing of solutions over their surface or when challenged with transmembrane potentials of $>\pm 500$ mV (see Fig. S1 in the Supporting Material).

tBLMs are fabricated sequentially, starting with a monolayer of sulfur groups that chemically attach to the gold surface and are covalently connected by linkers to hydrophobic groups that tether a subsequently formed lipid bilayer (Fig. 1 *A*). After the formation of the monolayer at the gold surface, a further solution of mobile lipids is incubated over the monolayer and, after 1–2 min, flushed with buffer to form a tethered lipid bilayer. In the current tBLM architecture, the sulfur-attached monolayer also contains spacers that laterally separate the tethers but do not directly interact with the membrane (Fig. 1 *A*). These spacers permit patches of mobile lipid to form within the tBLM, and other molecules, such as peptides or proteins, can be inserted into these lipid patches. For an excellent description of the structural details of sparsely tethered membranes, refer to Heinrich et al. (1).

In the tBLMs used here, 10% of the molecules are tethers and 90% are spacers. Using this tether/spacer ratio, tBLMs can be stored and remain functional for two to three months. This is in contrast to BLMs, which typically have lifetimes of the order of tens of minutes. Furthermore, BLMs are formed using solvents such as squalene or hexane, and they retain a significant fraction of the solvent within the hydrophobic interior of the bilayer (2). Such retained solvent can significantly alter the membrane properties. In solvent-exchanged tBLMs (3), however, the residual solvent levels can be essentially eliminated by aqueous rinsing after membrane formation (see Fig. S2). Forming a lipid bilayer over the tethered monolayer has most commonly been accomplished by employing fusion of liposomes onto the monolayer. This requires a high density of tethers to present a sufficiently hydrophobic monolayer surface to trigger the fusion of the liposomes with the tethers. Thus, fabrication of tBLMs is limited to tether/spacer group ratios of >70:30 (4). This approach has its limitations, as high tether densities have been shown to increase the membrane thickness (1), and the absence of sufficient patches of mobile lipid, created by the presence of spacer molecules in the monolayer, prevents the inclusion of compounds with a membrane-incorporated fraction exceeding ~1 kDa (calculated from the molecular volume

Submitted August 1, 2013, and accepted for publication November 15, 2013.

*Correspondence: c.cranfield@victorchang.edu.au

Charles G. Cranfield and Bruce A. Cornell contributed equally to this work.

Editor: Hagan Bayley.

0006-3495/14/01/0182/8 $2.00

http://dx.doi.org/10.1016/j.bpj.2013.11.1121

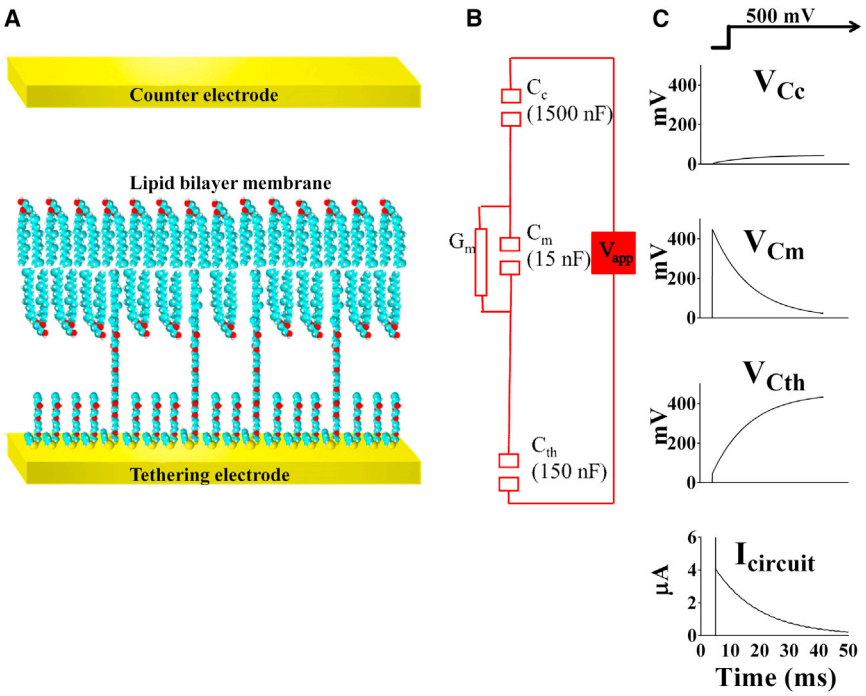

FIGURE 1 (*A*) Schematic diagram of a typical tBLM used in these experiments. (*B*) The equivalent circuit for the tBLM used here. For the electrode area of 2.1 mm^2, the actual values have been rounded to 1500 nF, 150 nF, and 15 nF to emphasize the 10-fold differences between the capacitances at each layer of the equivalent circuit. (*C*) Of the 500 mV step applied across the whole circuit, ~1%, or 0.004504 V, is initially expressed across the gold counterelectrode, C_c, ~10%, or 0.04504 V, across the tethering gold surface, C_{th}, and ~90%, or 0.4504 V, across the tethered membrane, C_m. The current response (*bottom plot*) initially shows a capacitive spike due to charging of C_m, C_{th}, and C_c. After this initial spike, the current slowly decays due to the charge being redistributed across C_{th} and C_c. When C_{th} and C_c are fully charged, the voltage across the membrane and the current will have decayed to zero. To see this figure in color, go online.

(v) assuming a 4-nm-thick membrane with an area/lipid of ~1 nm^2, where the molecular mass (m) is related to the density (ρ)). At tether densities of 10%, mobile lipid patches exist that are sufficiently large to permit the incorporation of membrane-embedded protein fractions possessing molecular masses up to ~40 kDa. Tether densities as low as 1% have also been shown to be stable for up to a month (Fig. S3) and can provide mobile lipid spaces that are sufficiently large to permit the insertion of membrane-bound protein fractions of up to ~300 kDa.

In the tBLM architecture described here, benzyl disulfide groups are employed as the sulfur chemistry for attaching the monolayer to the gold surface. Two families of benzyl-disulfide-terminated groups are used, one with a four-oxygen-ethylene-glycol group terminated by an OH group, included as the spacer molecule, and a second possessing an eight-oxygen-ethylene-glycol group terminated by a single C20 hydrophobic phytanyl chain, included as the tether. The C20 phytanyl chain incorporates into the inner leaflet of the subsequently formed lipid bilayer and tethers the bilayer to the gold surface.

Disulfide groups were chosen to minimize the effects of oxidation on the starting materials. Thiols tend to oxidize to disulfides on storage, which can cause the composition of the sulfur layer to vary. Disulfides do not suffer this problem. Here, the use of benzyl disulfides provides two additional advantages: they strengthen the weaker disulfide-gold bond through the dispersive attraction of the benzyl ring to the gold, and they act as an additional class of lateral spacer. The benzyl groups separate the gold attachment points at the sulfur-gold interface, creating volume that increases the mobility of ions adjacent to the gold. Ion mobility is a key to the use of tBLMs as a model for mimicking biological membranes, and the inclusion of an aqueous space between the gold surface and the tethered membrane provides a reservoir in which ions crossing the membrane can be stored or returned to the external solution (4–6). The fact that the spacer molecules used here are only half the length of the tether molecules creates an increased volume in the reservoir space, further increasing the mobility of ions in the reservoir and relaxing any packing restrictions experienced by the mobile lipid molecules within the tethered bilayer. The additional volume within the reservoir provided by the shorter spacer molecules also relieves steric interferences that might arise from protein moieties that project beyond the lipid bilayer. A challenge to studying the effects of transmembrane voltages across the tBLM arises from the isolation of the tBLM caused by the capacitive property of the gold surface to which the membrane is tethered. Any conductance across the tBLM will discharge the voltage across the membrane. In the architecture described here (Fig. 1 *B*), a fixed potential, V, applied to the tBLM circuit initially applies ~90% of V across the tBLM itself and ~10% of V across the tethering and return gold electrodes. The potential across the tBLM will decay over milliseconds to seconds, discharging the voltage to zero while simultaneously charging the tethering and return electrode capacitors to ~90% and ~10% of V, respectively. The voltages throughout this process reflect the inverse relationship of V with the capacitance values of the membrane, C_m, the tethering gold surface, C_{th}, and the return or counterelectrode, C_c (Fig. 1, *B* and *C*). Connecting the membrane directly to the voltage source, rather than through capacitive coupling by using redox active

electrodes might be thought of as an alternative approach. However, if redox active metals are used at the tethering electrode, the metal will ablate, causing a release of the tethers and a destabilization of the membrane. Furthermore, the use of a redox active counterelectrode will result in the release of metal ions into the bathing solution, potentially inactivating proteins or peptides being studied in the tBLM (7).

Using a tBLM with electrochemically inert gold electrodes, applied pulsed or ramped voltages will sustain transmembrane potentials for times in the range 1 – 100 ms across the membrane with typical conductances, G_m, of 100 – 1 μS cm^{-2}, respectively. From the I/V relationship in these time windows, studies can be undertaken of the voltage dependency of the insertion of peptides or ionophores into tBLMs, and of the intrinsic dependency on voltage of conduction of an ionophore once formed within the membrane.

The actual potential gradient across the tBLM can be quantitatively measured as a function of time from C_s, the effective series capacitance of C_{th} and C_c (Eq. 1), and the integrated current can be measured as a function of time flowing through G_m. At any instant, t, the loss of voltage across the tBLM, is matched quantitatively by the voltage increase across C_s.

$$C_s = \frac{C_c C_{th}}{(C_c + C_{th})}. \quad (1)$$

The voltage increase is given by Q/C_s where Q is the integral of the discharge current, I, accumulated to that point in time, t.

The ability of tBLMs to withstand high potentials provides a unique model for the study of the effects of electroporation membrane damage. Here, we propose that one result of electroporative failure is an increase in the membrane insertion efficiency of peptides. Peptides will spontaneously insert into lipid bilayers at zero applied potential, but the efficiency of insertion is increased by many orders of magnitude if membrane defects have been formed by electroporation. In this study, the insertion, assembly, and conduction of the antimicrobial peptide with a terminal glycine leucine-carboxyamide (PGLa) was observed while applying both pulsed and ramped potentials to tBLMs composed of 10% tethers and 90% spacers.

Using a unique alternating-current (AC) impedance spectroscopy method, the spontaneous insertion level of PGLa was measured at zero net transmembrane potential. This AC impedance spectroscopy method fits the impedance data in real time against an idealized single-capacitor-single-resistor circuit. This real-time modeling of the AC impedance data suggests that the origin of the loss of PGLa conduction at long times (hours) can be attributed to the formation of peptide aggregates forming in the membrane, which reduces the conduction per peptide and creates an inhomogeneous membrane.

MATERIALS AND METHODS

Tethered membrane formation

tBLMs were made using pre-prepared tethered benzyl-disulfide ethylene glycol T10 coated gold slides including 10% eight-oxygen-ethylene-glycol reservoir linkers with a C20 phytanyl group as tethers and 90% four-oxygen-ethylene-glycol reservoir linkers with a terminal OH group as spacers (SDx Tethered Membranes, Sydney, Australia; Fig. S4). A lipid bilayer was formed over the monolayer using a solvent-exchange technique that employs ethanol and water (3). Specifically, 8 μL of a 3 mM solution of a mobile lipid phase (70% zwitterionic C20 diphytanyl-ether-glycero-phosphatidylcholine lipid/30% C20 diphytanyl-diglyceride ether; DphPC) dissolved in ethanol was added to a 1 μL flow-cell chamber with a 500 μL connected liquid storage chamber. After an ~2 min incubation at 20°C, they were rinsed with 3 × 100 μL of phosphate-buffered saline (PBS) solution. Six such chambers were prepared in a single tethaPlate cartridge (SDx Tethered Membranes). Although many lipid solvents can be used (3,8), in most instances, the mobile lipids chosen to form the bilayer are soluble in ethanol. For lipids such as phosphatidylinositol that are insoluble in 100% ethanol, mixtures of chloroform, methanol, and water have been used (9).

The formation of the tBLMs was initially tested using a tethaPod (SDx Tethered Membranes) operating as described in the AC impedance spectroscopy section below. Typical results obtained for a lipid membrane were 0.8–1.2 μF cm^{-2}, and a conduction of 0.3–0.5 μS, for a 2.1 mm^2 electrode at 20°C and pH 7.2. To generate negatively charged lipid bilayers, the ethanolic mobile-lipid-phase lipid solution was mixed with 0–50% palmitoyl-oleoyl-phosphatidylglycerol (POPG).

AC impedance spectroscopy

The conductance and capacitance of the tethered membrane were determined using a tethaPod conductance reader (SDx Tethered Membranes), employing real-time modeling of the tBLM while operating as a swept-frequency ratiometric impedance spectrometer. A sequential 20 mV excitation was applied over the frequencies 1000, 500, 200, 100, 50, 20, 10, 5, 2.5, 1.25, 0.5, 0.25, and 0.125 Hz. The substantially capacitive load of a tBLM poses a challenging requirement for direct swept-frequency measurements of impedance over four decades of dynamic range, necessitating a high digital and analog resolution for the transimpedance amplifiers. These specifications were relaxed by employing a ratiometric measurement.

Ratiometric measure

By measuring the frequency dependence of the potential across the tBLM as a fraction of the applied potential across the tBLM plus a series reference element (Fig. 2), a frequency-dependent attenuation factor, ($f_{attn}(\omega)$), is defined. The series reference element comprises a fixed capacitor in parallel with a resistor with values chosen to be within a similar range to those anticipated in the test tBLM.

Fig. 2 shows a reference resistor-capacitor network in series with the test tBLM and the coupling capacitor (C_s). The change in load impedance, Z_1 (C_m, G_m, and C_s), with frequency has a similar dependence on frequency as the reference impedance, Z_2 (G_{ref} and C_{ref}). The ratio, $f_{attn}(\omega)$, therefore cancels the dominant load impedance change with frequency and emphasizes the relative differences between Z_1 and Z_2. This ratiometric approach results in a reduction by two orders of magnitude of the dynamic range required to read the impedance data,

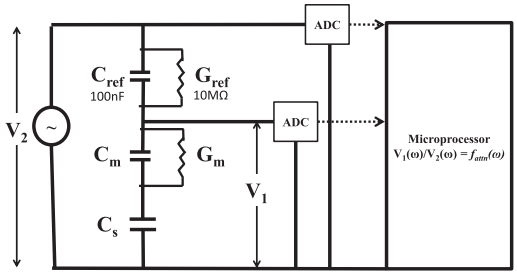

FIGURE 2 The equivalent circuit used for modeling the GOF values from impedance spectroscopy data. V_2 is a measure of the potential applied across the total network impedance, and V_1 is the resultant potential across the unknown load impedance. ADC, analog-to-digital converter.

eliminating the need for variable gain amplifiers and their associated software. As shown in Fig. 2, $f_{attn}(\omega)$ is fitted to C_m, G_m, and C_s using a microprocessor (ADuC70/24, Analog Instruments, Norwood, MA) according to

$$f_{attn(\omega)} = V_1/V_2 = I \times Z_1/I \times Z_2 = \left(\frac{(a_l\, d_l + b_l\, e_l)^2 + (d_l\, b_l\text{-}a_l\, e_l)^2}{\left(e_l^2 + d_l^2\right)}\right)^{0.5} \Bigg/ \left(\frac{(a_t\, d_t + b_t\, e_t)^2 + (d_t\, b_t\text{-}a_t\, e_t)^2}{\left(e_t^2 + d_t^2\right)}\right)^{0.5}, \quad (2)$$

where V_1 and V_2 are the potentials across the unknown load impedance, Z_1, and across the total network, Z_2, respectively, and I is the current through the network. The constants a, b, d, and e relate to the total (t) network impedance and the load (l) network impedance, whereas ω is the excitation frequency in radians/s. That is, for the total impedance network, including reference and unknown load,

$$a_t = 1 - \frac{\omega^2\left(C_m C_s + C_{ref} C_m + C_{ref} C_s\right)}{G_m G_{ref}}, \quad (3)$$

$$b_t = \omega\left(\frac{C_s}{G_{ref}} + \frac{C_s}{G_m} + \frac{C_{ref}}{G_{ref}} + \frac{C_m}{G_m}\right), \quad (4)$$

$$d_t = \omega^2 C_s\left(\frac{C_{ref}}{G_{ref}} + \frac{C_m}{G_m}\right), \quad (5)$$

and

$$e_t = \omega C_s - \left(\frac{\omega^3 C_{ref} C_m C_{th}}{G_{ref} G_m}\right). \quad (6)$$

And for the load network impedance (just unknown load):

$$a_l = 1, \quad (7)$$

$$b_l = \omega\left(\frac{C_s}{G_m} + \frac{C_m}{G_m}\right), \quad (8)$$

$$d_l = \frac{-\omega^2 C_s C_m}{G_m}, \quad (9)$$

and

$$e_l = \omega C_s. \quad (10)$$

Goodness of fit

The frequency dependence of the experimental attenuation factor is compared in real time during data acquisition with the calculated value according to Eq. 11. This approach tests the ability of the data to be mimicked by an idealized homogeneous conducting membrane modeled as a single membrane capacitance (C_m) in parallel with a single membrane conductance (G_m). The goodness of fit (GOF) function,

$$\mathrm{GOF} = \sum_{\omega = 2\pi 0.1}^{\omega = 2\pi 1000}\left(\left(f_{attn(\omega)_{\mathrm{exp\ erimental}}} - f_{attn(\omega)_{model}}\right)^2\right)^{0.5}, \quad (11)$$

is minimized within the tethaPod by adjusting C_{th}, C_m, and G_m while maintaining C_{ref} and G_{ref} fixed at $C_{ref} = 100$ nF cm^{-2} and $G_{ref} = 0.1$ μS. The RMS differences across all frequencies are summed, and if found to be ≤ 0.1, the values of G_m and C_m used in fitting the experimental data are reported.

A significant deviation of the data from the homogeneous membrane model indicates that the conductance arises from multiple C_m and G_m values, distributed at different sites across the membrane. This may occur physically from the aggregation of conductive pores into patches on a scale of tens to hundreds of nanometers, defined by the diffusion distance of a conductive ion during the period of the AC electrical excitation. An alternative interpretation is that an increase in GOF arises from a patchy loss of the membrane integrity due to, for example, detergent action or voltage breakdown causing well separated areas of membrane to degrade. Under the latter circumstances, however, the increase in the GOF is likely to be associated with a significant increase in the membrane capacitance (C_m) as more of the inner tethering surface capacitance is revealed. This was not generally observed here, suggesting that the reported effects arise from aggregation or clustering of the inserted peptides.

DC pulsed potential gradients

Voltage transients were applied across the tethered membrane circuit using an eDAQ ER466 Potentiostat in conjunction with eScope software (eDAQ) operating with a bandwidth of 100 kHz. Rectangular voltage pulses of 20 ms duration were applied, increasing from 0 mV to $\pm$300 mV in 50 mV increments (see Fig. 5 *A*). Simultaneous current recordings were averaged over 16 sweeps with a repetition delay of 1 s. Potentials are defined as the potential of the tethered gold electrode relative to the return electrode. After all potential measurements up to $\pm$300 mV, any lasting damage caused to the tBLMs was determined using AC impedance spectroscopy. To induce lasting electroporation damage, three sequences of 20 ms pulses were applied, with 10 steps/sequence, from 0 to $\pm$500 mV in $\pm$50 mV increments.

Ramped potential gradients

Ramped potentials were applied using EChem v4.0.13 software (eDAQ). Voltage ramps of $\pm$100 V/s were applied for 3 ms, to a peak volage

of ±300 mV. Voltage increases occurred stepwise in 100 × 0.05 ms steps (i.e., ±5 mV/0.05 ms). For each 0.05 ms step, current recordings were averaged over 0.01 ms intervals after the voltage increment. It was important to limit the time course of the potential ramps to less than a few milliseconds to ensure that the transmembrane potential closely matched the applied potential ramp.

Antimicrobial peptide PGLa synthesis

The peptide GMASKAGAIAGKIAKVALKAL-amide (peptidyl-glycine-leucine-carboxyamide (PGLa)) was synthesized using standard solid-phase Fmoc protocols (10,11) on an Applied Biosystems (Carlsbad, CA) 433A instrument and purified using reverse-phase HPLC employing a water/acetonitrile gradient and a C18 column, as described in detail by Afonin et al. (12). The bacterial toxin channel α-hemolysin was purchased from Sigma-Aldrich (St. Louis, MO).

Equivalent circuit modeling

The electrical equivalent circuit of the 2 mm^2 tethered membrane experimental system for both AC impedance spectroscopy and DC amperometry is shown in Fig. 1 *B*. The response of this circuit to any applied potential may be simulated using the freeware simulation package 5SPICE (Andresen Software, Oakland, CA). The circuit comprises two coupling capacitors (~70 $\mu F\ cm^{-2}$ return electrode (C_c); ~7 $\mu F\ cm^{-2}$ gold tethering electrode (C_{th})) and a 0.8–1.2 $\mu F\ cm^{-2}$ membrane capacitance (C_m). In addition, it contains a conductor (G_m), representing the membrane conduction, whose value may be adjusted to represent the conductivity of an ion channel or, in the absence of an ion channel, the baseline conduction of the tethered lipid bilayer. Circuit responses across all elements for pulsed and ramped applied potentials are shown in Fig. 1 *C* (see also Fig. 6 *B*).

RESULTS

Effect of PGLa addition on conductance measured by AC impedance spectroscopy

The tethaPod reader provides a continuous recording of G_m and C_m based on fitting the impedance spectrum to a single idealized G_m-C_m network together with a GOF value indicating the quality of the fit of the data to this simple equivalent circuit. Fig. 3 *A* shows G_m during the addition of 10 μL of varying concentrations of PGLa in PBS. Fig. 3 *B* is the peak conduction in Fig. 3 *A*, which shows a nonlinear relationship with PGLa concentration. Fig. 3 *C* shows the conductance after the addition of 30 μM PGLa to membranes that contain 0 – 50% of the negatively charged phospholipid POPG in PC lipids. The peak conductance progressively increased >30-fold with a progressive increase in the POPG concentration. However, at longer times, in response to PGLa addition in either PC or POPG-enriched tBLMs, G_m reversed and decreased. The bacterial toxin α-hemolysin is included as a control in Fig. 3 *C*. Unlike the effect of PGLa on conductance, α-hemolysin caused a conductance increase that remained high, and even slightly increased over 5 h.

Membrane heterogeneity

With the rise in conduction due to the addition of PGLa there is an associated and progressive increase in the GOF beyond 0.1, indicating failure of the single-C_m and single-G_m network model to describe the impedance characteristics of the membrane. This suggests a progressively more heterogeneous distribution of conductive PGLa within the membrane as the conduction increases. The origin of this heterogeneity may arise from PGLa self-assembling and/or forming mixtures with the anionic lipids (13). As the conduction decreased, the GOF also decreased, suggesting that the reduction in G_m was associated with an annealing of the heterogeneities giving rise to a more homogenous and less conducting state. Salnikov and Bechinger (14) reported that multiple conformations of PGLa are adopted within a lipid bilayer at high concentrations of PGLa. These multiple conformations may reflect states with different conductivity such as those seen here. The bacterial toxin α-hemolysin similarly causes the GOF to increase with conduction, but with α-hemolysin, the increased conduction and GOF are maintained over many hours (Fig. 3 *D*). Modeling the effect of peptide insertion on the heterogeneity of membrane

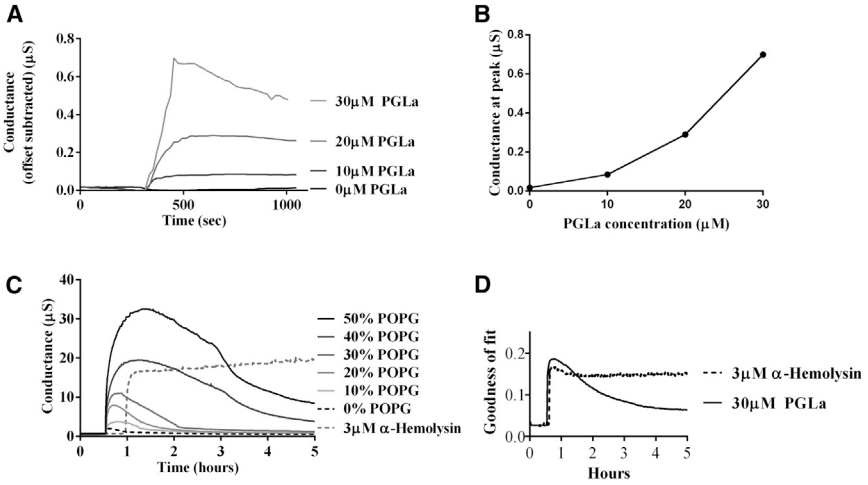

FIGURE 3 (*A*) AC impedance spectroscopy conductance readings in response to varying concentrations of PGLa in zwitterionic lipids over time. All readings were baseline-conductance offset from the time point of addition of a 10 μL PGLa sample or a blank PBS control. (*B*) Peak conductance readings from *A* for each PGLa concentration. (*C*) AC impedance spectroscopy conductance readings of 30 μM PGLa added to tBLMs containing various amounts of negatively charged POPG lipids. PGLa responses are compared to the addition of 3 μM α-hemolysin to a POPG-free tBLM. (*D*) AC impedance GOF calculations in response to PGLa and α-hemolysin over time.

conduction can be pursued using more complex constant-phase-element models (15), but is beyond the scope of the current discussion.

Membrane capacitance

Fig. 4 shows C_m as a function of percentage POPG content in DphPC tBLMs. The incorporation of POPG into the tBLM is evident from the linearity of the capacitance change with the nominal POPG content.

Electroporation

Fig. 5 *A* shows applied voltage steps (V_{app}) in the range 0 to $\pm$300 mV in 50 mV steps across a tBLM containing 40% POPG lipids. The current traces possess an initial short-lived high-amplitude spike, followed by a series of low-amplitude exponential decays that continued beyond the measurement period of 20 ms. These current traces reflect the inherent charging current of C_s through G_m. The integral of this current is a measure of the charge ($Q_{(t)}$) being transferred across the membrane. The voltage across the membrane, $V_{m(t)}$, is thus given by the applied voltage minus $Q_{(t)}/C_s$:

$$V_{m(t)} = V_{app} - \frac{Q_t}{C_s}. \tag{12}$$

At voltages >~150 mV the current traces diverge from a linear dependence on voltage, suggesting an increased current due to electroporation (Fig. 5 *B*). This is more evident in the presence of the peptide PGLa, suggesting that electroporation assists with peptide insertion. Fig. 5 *C* shows the normalized $V_{m(t)}$ at $V_{app} = 50$ mV and 300 mV. The electroporation caused by $V_{app} = 300$ mV results in a more rapid decay of $V_{m(t)}$ than with $V_{app} = 50$ mV.

The application of a linear voltage ramp in the same range of 0 to $\pm$300 mV showed a current trace reflecting a dependency of electroporation on voltage similar to that seen with the application of pulsed potentials. A 5SPICE simulation of ramped potentials across the equivalent circuit is shown in Fig. 6 *B*. The simulated step in current with the onset of the potential ramp closely matches the experimental result, confirming the AC impedance measurement of $C_m = 1.19$ μF cm^{-2}. In Fig. 6 *C*, the current traces with and without PGLa are compared with the equivalent circuit. However, in this case, the tBLM had been subjected to multiple voltage steps between +500 mV and −500 mV, resulting in lasting electroporation damage that potentiated the effects of PGLa on the transmembrane current.

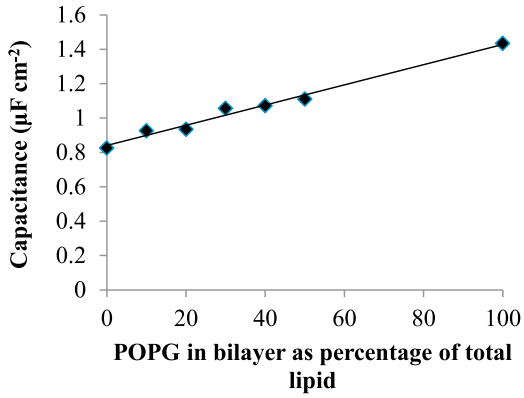

FIGURE 4 Increased capacitance caused by incorporating the anionic POPG into the lipid bilayer.

DISCUSSION

The tBLM architecture employed here, which incorporates sparsely separated tethering sites, permitted the incorporation and formation of conductive membrane defects induced by PGLa. The tethered membranes could be prepared incorporating up to 100% charged POPG lipids, allowing the study of the influence of charged lipids that mimic bacterial membranes.

Two approaches have been applied here to study the incorporation of the antimicrobial peptide PGLa into tBLMs. A low-voltage (20 mV) AC impedance spectroscopy reading provided measures of basal membrane conduction and capacitance, and a high-voltage (0 to $\pm$300 mV) pulsed and ramped amperometry approach provided measures of the electroporation voltage dependency of the membrane catalyzing PGLa incorporation and conduction. The nonlinearity of the peak conduction as a function of PGLa concentration suggests that some level of oligomerization of PGLa is required to form a conductive pore, as has been suggested previously for similar antimicrobial peptides (16,17).

The conductance increase observed upon the addition of PGLa to the membrane correlates with an increased GOF value. This may arise from the formation of families of conductive PGLa aggregates possessing a number of different membrane topologies (14,18). However, even though the membrane conduction is heterogeneous, the capacitance remained substantially unaltered, indicating that the membrane remained intact (see Fig. S5). The speed at which the impedance spectrum changes upon the addition of PGLa can have an impact on the apparent estimate of GOF. Transients in conduction that are faster than the sweep rate from 1000 Hz to 0.1 Hz (~20 s^{-1}) will result in GOF estimates that will yield flawed measures of G_m, C_m, and C_c. In the data presented here, such transients are evident immediately upon the addition of PGLa, but are relaxed within <1 min as the rate of change of conductance decreases below the data acquisition rate (data not shown).

After the application of a 20 ms DC potential pulse of increasing magnitude, the resultant current decay could be decomposed into multiple components. The transmembrane potential is significantly reduced after 15–20 ms as the

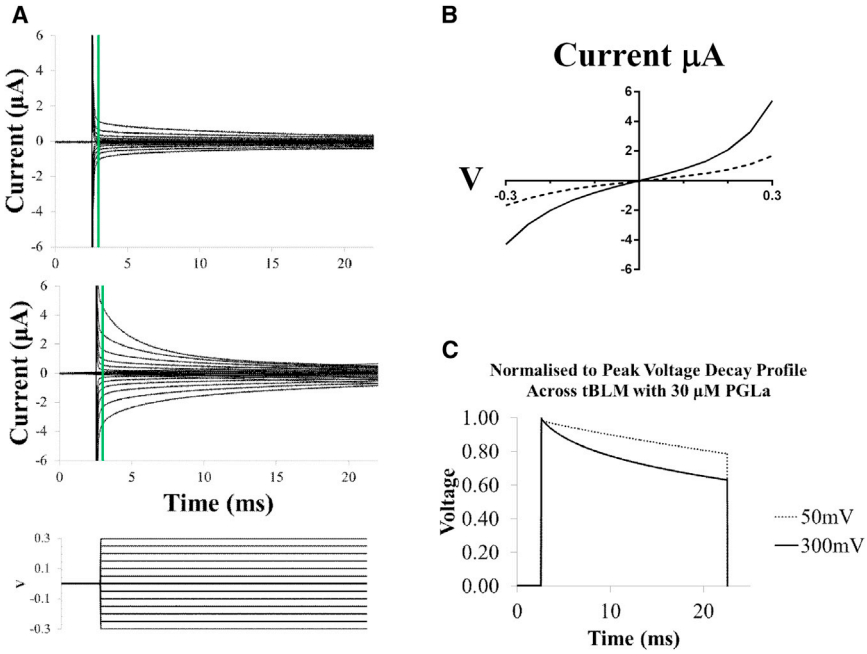

FIGURE 5 (*A*) Voltage-clamp data measured from a tethered lipid bilayer containing 40% negatively charged POPG lipids in the absence (*upper*) and presence (*middle*) of 30 μM PGLa peptide. For the lower plot, 50 mV voltage steps were applied for 20 ms. Recordings at each voltage step are the average of 16 sweeps. Green lines indicate time periods of 0.3 ms post pulse initiation. (*B*) I/V plot of responses recorded 0.3 ms post pulse initiation for control (*dashed line*) and in response to 30 μM PGLa (*solid line*). At voltages >~150 mV, the current traces become nonlinear, suggesting an increased current due to electroporation. This is clearly evident in the PGLa case, indicating that electroporation assists with peptide insertion. (*C*) By integrating the data from the pulsed traces in *A* it is possible to calculate the charge across the membrane, and thereby the voltage across the membrane. The plot in *C* represents the normalized-to-peak voltage decay across the membrane to an applied 20 ms pulse of 300 mV compared to a 50 mV pulse of the same duration. Because of electroporation, a more rapid decay in voltage across the membrane is seen due to decreased resistance across the tBLM than at lower voltages. To see this figure in color, go online.

coupling capacitors C_{th} and C_c are charged through the membrane conductance, G_m. At low voltages (<~ $\pm$ 150 mV), the dominant feature is a rapidly decaying spike (0.5 ms) arising from a large displacement current charging both the membrane and coupling capacitors. At longer times, a current consistent with the measured AC conductance levels persisted beyond 20 ms. At higher voltages (> $\pm$ 150 mV), an additional current component decaying over 15 ms became evident and was identified with electroporation defects caused by the voltage pulse sustaining the membrane voltage above a critical electroporation threshold.

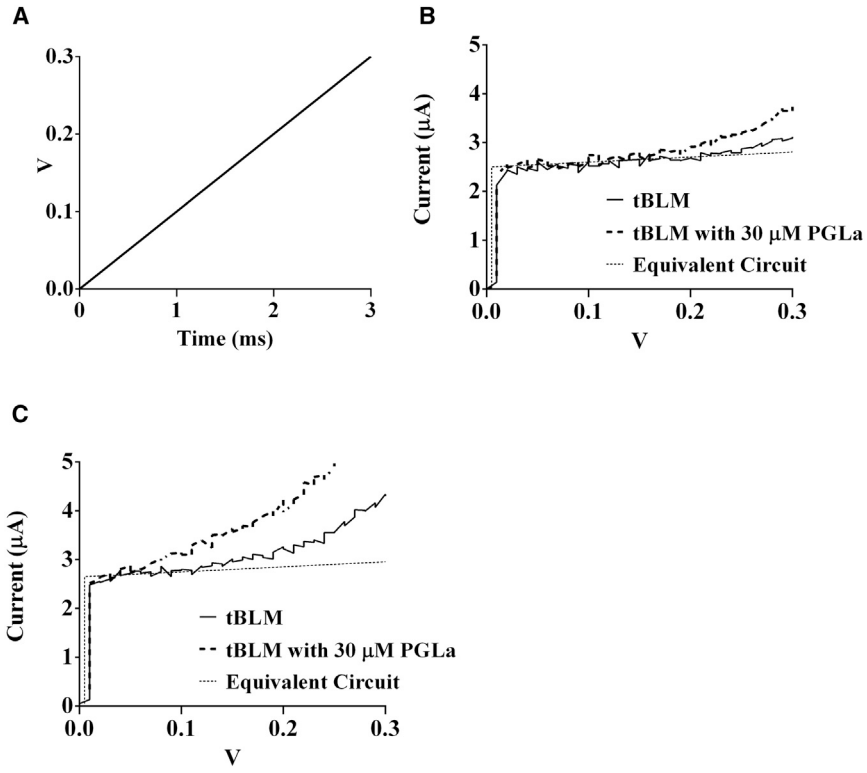

FIGURE 6 (*A*) Ramped voltage pattern applied to the tBLM to measure the electroporation threshold. (*B*) The resultant current in response to the voltage ramp illustrates the electroporation threshold, as well as the insertion of PGLa compared with the experimental current and a 5SPICE simulation of the equivalent circuit of a sealed tBLM. The initial rise in current seen in both the experimental and simulated traces confirms the capacitance readings obtained using AC impedance spectroscopy of C_m = 1.19 μF cm^{-2}. (*C*) A further tBLM after exposure to three sequences of 20 ms pulses from 0 to $\pm$500 mV in $\pm$50 mV increments, subsequently read using the same ramped potential as in *B*. It should be noted that the signal/noise ratio of the currents measured arising from the ramped potentials in Fig 6, *B* and *C*, is ~1–2 orders of magnitude lower than that from the swept-frequency AC measures.

In the presence of PGLa, similar characteristics were observed, except that with the onset of electroporation the current was significantly greater and the long-term conduction remained higher. This is interpreted as the electroporation facilitating the incorporation of PGLa, which then results in an increase in long-term membrane conduction.

An electroporation threshold potential may be determined more readily from the ramped potential data obtained with and without PGLa (Fig. 6 *B*). Voltages in excess of ~150 mV appeared to form electroporation defects in the membrane that facilitate the formation of PGLa-induced pores. Multiple applications of the potential gradient in excess of ± 200 mV were required to achieve a sustained high conduction arising from peptide insertion into the tBLM. With minimal electroporation damage, the raised conduction levels returned to near their initial values. However, with increased electroporation damage, the rise in conduction was sustained (Fig. 6 *C*). This suggests that electroporative pore formation initially causes a reversible insertion of PGLa, but that with repeated application of the ramped potential, a sustained conduction is maintained; thus, the membrane including PGLa appears to adopt a new configuration that remains within the membrane when the applied potential is removed.

CONCLUSIONS

In this study, we describe a tBLM architecture and AC impedance spectroscopy technique that allows a rapid measure of the insertion and aggregation of pore-forming peptides such as PGLa. The stability of the tethered lipid bilayers also permits the use of high-voltage DC amperometry to study electroporation-induced defects in the membrane that catalyze the insertion of PGLa.

SUPPORTING MATERIAL

Five figures are available at http://www.biophysj.org/biophysj/supplemental/S0006-3495(13)02379-5.

Bruce Cornell is a shareholder, and Sonia Carne an employee, of Surgical Diagnostics. Paul Duckworth is an employee of eDAQ. We gratefully acknowledge Parvesh Wadhwani, Andrea Eisele, and Kerstin Scheubeck (Karlsruhe Institute of Technology) for providing the PGLa peptide. We also acknowledge Heba Alkhamichi and Hedayetul Islam for technical support.

This study was supported by the National Health & Medical Research Council (NH&MRC) of Australia (Grant 635525) and the Deutsche Forschungsgemeinschaft Center for Functional Nanostructures (TP E1.2).

REFERENCES

1. Heinrich, F., T. Ng, …, M. Lösche. 2009. A new lipid anchor for sparsely tethered bilayer lipid membranes. *Langmuir.* 25:4219–4229.
2. Cornell, B. A. 2002. Memembrane-based biosensors. *In* Optical Biosensors: Present and Future. F. Ligler and C. A. R. Taitt, editors. Elsevier Science, Amsterdam, pp. 457–459.
3. Cornell, B. A., V. L. B. Braach-Maksvytis, …, R. J. Pace. 1997. A biosensor that uses ion-channel switches. *Nature.* 387:580–583.
4. Krishna, G., J. Schulte, …, P. D. Osman. 2003. Tethered bilayer membranes containing ionic reservoirs: selectivity and conductance. *Langmuir.* 19:2294–2305.
5. Krishna, G., J. Schulte, …, P. D. Osman. 2001. Tethered bilayer membranes containing ionic reservoirs: the interfacial capacitance. *Langmuir.* 17:4858–4866.
6. Cornell, B. A., G. Krishna, …, L. Wieczorek. 2001. Tethered-bilayer lipid membranes as a support for membrane-active peptides. *Biochem. Soc. Trans.* 29:613–617.
7. Ghandour, W., J. Hubbard, …, R. Poole. 1988. The uptake of silver ions by *Escherichia coli* K12: toxic effects and interaction with copper ions. *Appl. Microbiol. Biotechnol.* 28:559–565.
8. McGillivray, D. J., G. Valincius, …, M. Lösche. 2007. Molecular-scale structural and functional characterization of sparsely tethered bilayer lipid membranes. *Biointerphases.* 2:21–33.
9. Shekhar, P. 2012. Neutron reflectometry from interfacial molecular architectures: structural modeling and application to sparsely tethered bilayer lipid membranes. PhD thesis. Carnegie Mellon University, Pittsburgh, Pennsylvania.
10. Chang, C.-D., and J. Meienhofer. 1978. Solid-phase peptide synthesis using mild base cleavage of N α-fluorenylmethyloxycarbonylamino acids, exemplified by a synthesis of dihydrosomatostatin. *Int. J. Pept. Protein Res.* 11:246–249.
11. Fields, G. B., and R. L. Noble. 1990. Solid phase peptide synthesis utilizing 9-fluorenylmethoxycarbonyl amino acids. *Int. J. Pept. Protein Res.* 35:161–214.
12. Afonin, S., R. W. Glaser, …, A. S. Ulrich. 2003. 4-fluorophenylglycine as a label for 19F NMR structure analysis of membrane-associated peptides. *ChemBioChem.* 4:1151–1163.
13. Wadhwani, P., R. F. Epand, …, R. M. Epand. 2012. Membrane-active peptides and the clustering of anionic lipids. *Biophys. J.* 103:265–274.
14. Salnikov, E. S., and B. Bechinger. 2011. Lipid-controlled peptide topology and interactions in bilayers: structural insights into the synergistic enhancement of the antimicrobial activities of PGLa and magainin 2. *Biophys. J.* 100:1473–1480.
15. Chang, W. K., W. C. Wimley, …, M. Merzlyakov. 2008. Characterization of antimicrobial peptide activity by electrochemical impedance spectroscopy. *Biochim. Biophys. Acta.* 1778:2430–2436.
16. Yang, L., T. M. Weiss, …, H. W. Huang. 2000. Crystallization of antimicrobial pores in membranes: magainin and protegrin. *Biophys. J.* 79:2002–2009.
17. Zasloff, M. 2002. Antimicrobial peptides of multicellular organisms. *Nature.* 415:389–395.
18. Glaser, R. W., C. Sachse, …, A. S. Ulrich. 2005. Concentration-dependent realignment of the antimicrobial peptide PGLa in lipid membranes observed by solid-state 19F-NMR. *Biophys. J.* 88:3392–3397.